RSC Advances

PAPER

View Article Online
View Journal | View Issue

Cite this: *RSC Adv.*, 2021, **11**, 5865

Phosphonated mesoporous silica nanoparticles bearing ruthenium complexes used as molecular probes for tracking oxygen levels in cells and tissues†

Yui Umehara,[a] Yu Kimura,[a] Freddy Kleitz,[b] Tatsuya Nishihara,[c] Teruyuki Kondo *[a] and Kazuhito Tanabe *[c]

Molecular oxygen plays an important role in living organisms. Its concentration and fluctuation in cells or tissues are related to many diseases. Therefore, there is a need for molecular systems that can be used to detect and quantify oxygen levels *in vitro* and *in vivo*. In this study, we synthesized phosphonated mesoporous silica nanoparticles bearing ruthenium complexes in their pores (pM-Rus) and evaluated their photophysical and biological properties. The pM-Rus were highly soluble in water and showed robust phosphorescence under hypoxic conditions, while the addition of oxygen suppressed this emission. Cellular experiments revealed that pM-Rus with a size of 100 nm showed efficient cellular uptake to emit phosphorescence in hypoxic cells. In addition, pM-Rus have negligible toxicity to cells due to the blockage of direct contact between ruthenium complexes and intracellular biomolecules and the deactivation of singlet oxygen ($^1O_2$) generated by photoexcitation of ruthenium complexes before leaking out of the pores. Animal experiments confirmed that pM-Rus showed robust emission at hypoxic regions in mice. Thus, pM-Rus are promising oxygen probes for living systems.

Received 15th October 2020
Accepted 25th January 2021

DOI: 10.1039/d0ra08771h

rsc.li/rsc-advances

Introduction

Oxygen is an essential molecule for living organisms, as it is related to many chemical reactions in biological systems including the generation of energy and maintenance of the redox balance.[1] The supply and concentration of oxygen are strictly controlled,[2,3] and oxygen deficiency is related to many diseases, such as cardiovascular ischemia,[4,5] inflammatory disease,[6] and the formation of solid tumors.[7,8] Therefore, monitoring of oxygen partial pressure and its fluctuation is important for understanding these diseases and for their treatment.

To monitor and detect oxygen levels in cells and tissues in real time, many techniques such as the use of fluorophores,[9–13] radioactive species,[14] oxygen-responsive electrodes,[15] and magnetic resonance imaging (MRI) probes have been developed.[16,17] Among these, phosphorescent imaging using metal complexes is one of the most useful methods for visualizing the oxygen concentration and its fluctuation. Phosphorescence, which refers to emission from a triplet excited state of molecules, is rapidly quenched by energy transfer to molecular oxygen, so that the intensity and lifetime of phosphorescence are dependent on the oxygen concentration in the solution. Conventionally, phosphorescent metal complexes (*e.g.*, ruthenium (Ru),[18–21] and iridium,[22–24] and porphyrin–metal complexes[25,26]) have been reported as oxygen probes. These probes show robust emission under hypoxic conditions and have been applied to the molecular imaging of hypoxic regions in mice. However, there are two problems associated with these complexes; the molecules themselves are cytotoxic, and singlet oxygen ($^1O_2$) is generated by energy transfer from the excited metal complex to molecular oxygen. $^1O_2$ is a reactive oxygen species (ROS) that can oxidize many molecules in living cells to show a toxic effect.

To overcome these problems, we designed functional mesoporous silica nanoparticles (MSNs). Mesoporous materials have nano-sized (2–50 nm) pores. We recently demonstrated that $^1O_2$ generated in these pores was rapidly deactivated and could not leak out from the pores.[27] More recently, we prepared MCM-41-type MSNs tethered to phosphorescent Ru complexes inside their pores (MSN-Rus) and used them to visualize oxygen

[a]*Department of Energy and Hydrocarbon Chemistry, Graduate School of Engineering, Kyoto University, Nishikyo-ku, Kyoto, 615-8510, Japan. E-mail: teruyuki@scl.kyoto-u.ac.jp; Fax: +81-75-383-2504; Tel: +81-75-383-7055*

[b]*Department of Inorganic Chemistry – Functional Materials, Faculty of Chemistry, University of Vienna, Währinger Straße 42, A-1090, Vienna, Austria*

[c]*Department of Chemistry and Biological Science, College of Science and Engineering, Aoyama Gakuin University, 5-10-1 Fuchinobe, Chuo-ku, Sagamihara, 252-5258, Japan. E-mail: tanabe.kazuhito@chem.aoyama.ac.jp; Fax: +81-42-759-6493; Tel: +81-42-759-6229*

† Electronic supplementary information (ESI) available. See DOI: 10.1039/d0ra08771h

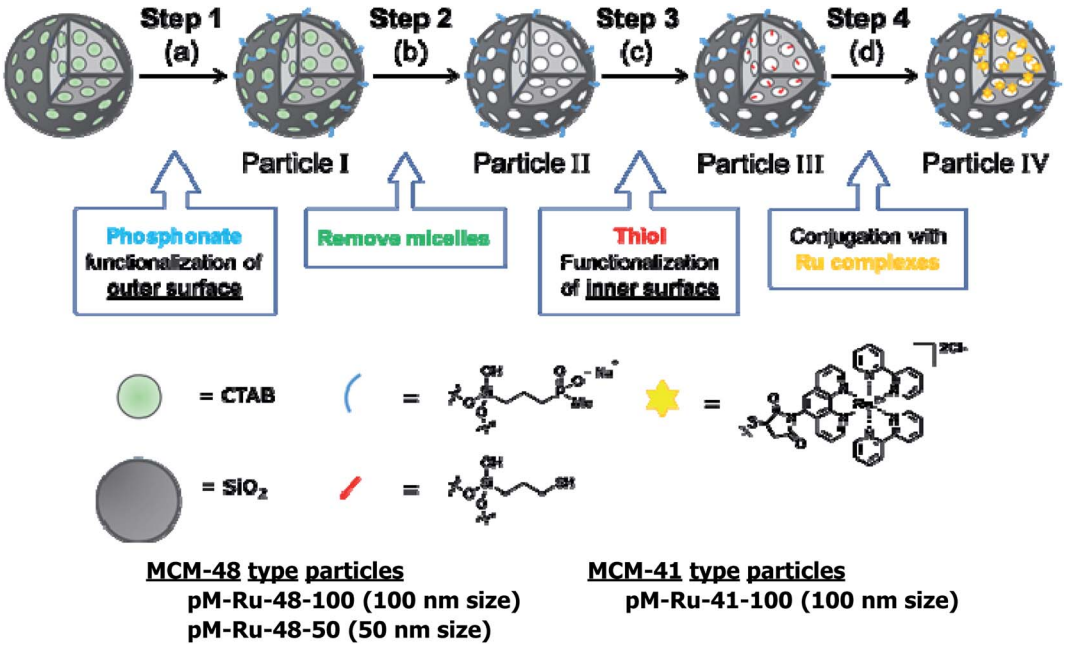

Scheme 1 Reagents and conditions: (a) THMP, HCl, H_2O, 100 °C, 18 h; (b) HCl, EtOH, 80 °C, 1 h; (c) MPTS, toluene, 110 °C, 18 h; (d) Ru complex, DMSO, sodium phosphate buffer (pH 8.0), r.t., 18 h.

fluctuation *in vitro* and *in vivo*.[28] In the MSN-Rus, almost all of the ruthenium complexes were covalently attached in the silica mesopores, and therefore, their contact with intracellular biomolecules was limited, leading to negligible cytotoxicity. In addition, the MSN-Rus generated $^1O_2$ upon photoirradiation inside the pores. However, the $^1O_2$ in the MSN-Rus did not exhibit cytotoxic effects due to its deactivation in the pores. Thus, MSN-Rus were promising molecular probes for detecting oxygen levels in cells without any cytotoxicity. However, these conventional MSN-Rus were too large (400–500 nm) to circulate in blood vessels in a living body. When they were administered, they were trapped by blood proteins and rapidly excreted by the liver. In addition, MSN-Rus showed low colloidal dispersibility in water, and thus are not suitable for intravenous injection. To overcome these problems, in the present study, we newly synthesized Ru complex-tethered MCM-41- and MCM-48-type MSNs with a smaller size (*ca.* 100 nm). We expected that they might show good biocompatibility and longer retention in blood.[29] Further, we established the selective modification procedures of external surface of nanoparticles by phophonate (pM-Rus) to make the particles more hydrophilic and improve their colloidal stability. Consequently, pM-Rus showed preferable properties for biological application as an oxygen probe.

Results and discussion

The synthesis of pM-Rus was conducted according to a previously reported procedure (Scheme 1).[30,31] Initially, we synthesized MSNs that were phosphonate-functionalized on their surface (particle I) and then the surfactant micelles were removed (particle II, see also Table S1†). Subsequently, we functionalized their inner surface by thiol groups (particle III). Finally, Ru complexes were incorporated into the pores of MSNs (particle IV). We prepared two sizes of MCM-48-type MSNs (pM-

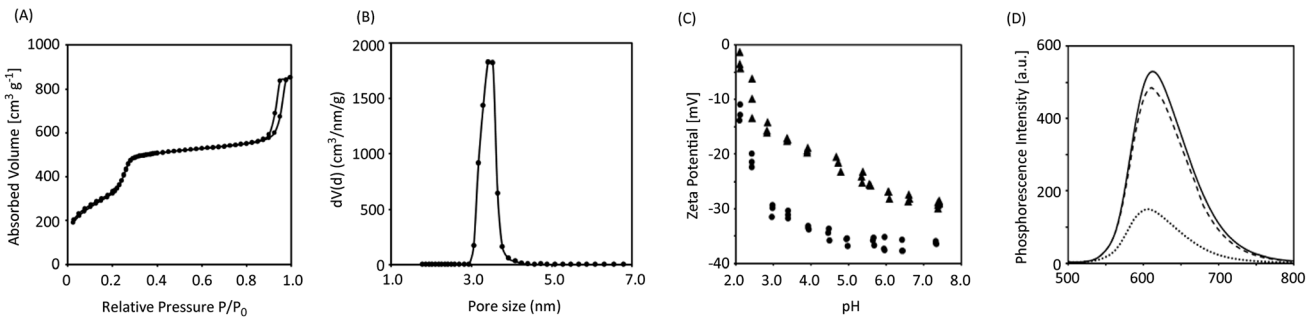

Fig. 1 (A) N_2 physisorption isotherms of pM-Ru-48-100. The analysis was conducted at −196 °C. (B) Pore size distribution analysis of pM-Ru-48-100. (C) The effect of pH on zeta potentials of M-Ru-48-100 (triangle) and pM-Ru-48-100 (circle). (D) Phosphorescence spectra of pM-Ru-48-100 (solid line), pM-Ru-41-100 (dashed line) and pM-Ru-48-50 (dotted line). The spectra were measured with excitation at 450 nm.

Table 1 Amount of ruthenium (Ru) complex and Stern–Volmer coefficient (K_{SV}) of the nanoparticles

	pM-Ru-48-100	pM-Ru-41-100	pM-Ru-48-50	M-Ru-48-100	M-Ru-41-100	M-Ru-48-50
Amount of Ru complex [μmol g^{-1}]	60	40	3.5	12	35	4.1
K_{SV} [M^{-1}]	4346	4148	4811	2843	3621	3341

Table 2 Basic parameters of nanoparticles obtained from DLS and physisorption analysis

	Size (DLS) [nm]	Surface area [m^2 g^{-1}]	Pore volume [cm^3 g^{-1}]	Mean pore size [nm]
pM-Ru-48-100	94.8	1.22×10^3	1.26	3.5
pM-Ru-41-100	127.2	6.40×10^2	0.74	3.2
pM-Ru-48-50	66.4	1.08×10^3	1.56	3.5

Ru-48-100 of size 100 nm and pM-Ru-48-50 of size 50 nm) and an MCM-41-type material of size 100 nm (pM-Ru-41-100). We also prepared control nanoparticles without surface modifications by phosphonate (MCM-48-type: M-Ru-48-100 of size 100 nm and M-Ru-48-50 of size 50 nm; MCM-41-type: M-Ru-41-100 of size 100 nm). To confirm that they were still porous after modification, all pM-Rus were subjected to physisorption analysis. The representative behavior of pM-Ru-48-100 is shown in Fig. 1A (see also Fig. S1†). The steep uptake at low P/P_0 in the isotherms is associated with adsorbent–adsorptive interactions in narrow mesopores. Pore sizes were estimated by using nonlocal density functional theory (NLDFT) to be 3.4, 3.1 and 3.5 nm for pM-Ru-48-100, pM-Ru-41-100 and pM-Ru-48-50, respectively (Fig. 1B and S1B†). Thus, the nanoparticles maintained a certain porosity even after modification. The XRD

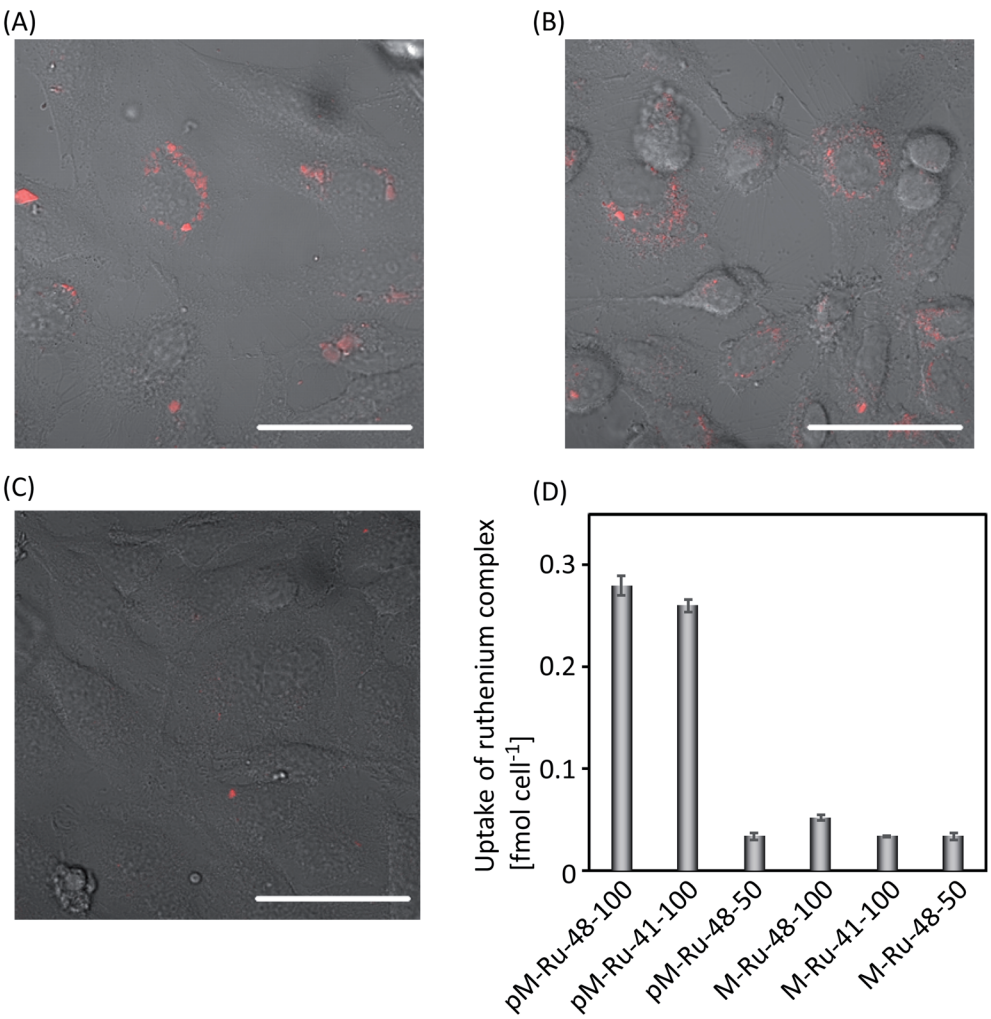

Fig. 2 (A–C) Confocal microscopic images of HeLa cells after addition of pM-Ru-48-100 (A), pM-Ru-41-100 (B) and pM-Ru-48-50 (C). The cells were incubated with pM-Rus (0.02 mg mL^{-1}) for 24 h and the cell images were obtained under hypoxic conditions. Scale bar: 50 μm. (D) The amount of ruthenium complexes in HeLa cells estimated by ICP MS analysis.

patterns of pM-Rus show preservation of typical MCM-48- and MCM-41-type structures (Fig. S2†). In addition, a more negatively charged surface was observed for pM-Rus than for MSNs without modification (M-Rus) in the measurement of zeta potentials of the nanoparticles, indicating that the particle surfaces were modified by phosphonate (Fig. 1C and S1C†). The pM-Rus were negatively charged even under neutral pH conditions due to these modifications. The obtained particles, pM-Rus, have good dispersity in water as well as phosphate-buffered solution (Fig. S3†). We also confirmed the modification of nanoparticles by Ru complexes by the measurement of emission spectra. As shown in Fig. 1D, a robust phosphorescence emission at around 610 nm was observed for all pM-Rus. The number of tethered Ru complexes was estimated to be from 3.5 to 60 μmol g^{-1} by atomic absorbance spectroscopy (Table 1). TEM/EDX revealed that the nanoparticles had phosphonate and Ru complexes on their surface and their pores, respectively (Fig. S4†). The sizes of the particles were estimated by DLS measurements to be 95, 127 and 66 nm for pM-Ru-48-100, pM-Ru-41-100 and pM-Ru-48-50, respectively (Table 2). We also measured the IR spectra of nanoparticles. We confirmed the band around 2600 cm^{-1}, which was attributed to thiol groups in particle III, while introduction of Ru complexes resulted in a disappearance of the band. Thus, Ru complexes were linked *via* thiol groups. In addition, we observed the band around 1700 cm^{-1} for complex IV, which was attributed to the C=O stretching vibration of maleimide units in ruthenium complexes (Fig. S5†).

We next evaluated the oxygen-dependent phosphorescence of pM-Rus. While the MSNs phosphoresced robustly under hypoxic conditions, the addition of molecular oxygen resulted in a suppression of their emission. The response of phosphorescence intensity to the oxygen concentration obeyed a Stern–Volmer relationship. The oxygen concentration was proportional to the ratio of the phosphorescence intensities of each pM-Ru (I_0/I, where I_0 is the intensity under anoxic conditions and I is the intensity under the indicated oxygen concentration). The Stern–Volmer constants (K_{SV}), which are an index of the responsiveness to the oxygen concentration, were calculated and are summarized in Table 1 (see also Fig. S6†). All of the pM-Rus had K_{SV} values higher than those of M-Rus without phosphonate groups on their surface. This is probably due to the high dispersity of particles in water, which gives oxygen molecules easy access to the inner Ru complexes.

We next compared the cellular uptake and behaviors of pM-Rus. Each set of particles was incubated with HeLa cells, and their emission was observed by confocal microscopy and a microplate reader. As shown in Fig. 2A and B, the bright emission of the Ru complex was observed from cells incubated with pM-Ru-48-100 and pM-Ru-41-100 of size 100 nm, while weak emission was observed from those incubated with pM-Ru-48-50 of size 50 nm (Fig. 2C). In addition, we determined the total amount of Ru complexes in the cells. After HeLa cells were incubated in the presence of pM-Rus, we treated cells with HNO_3. ICP-MS measurement of the resulting samples estimated the accumulation of Ru complexes in the cells to be 0.28, 0.03, and 0.26 fmol per cell for pM-Ru-48-100, pM-Ru-48-50 and pM-Ru-41-100, respectively. Thus, pM-Rus of size 100 nm were effectively internalized into cells, while smaller particles appeared to have low cellular uptake. We also evaluated the internalization of M-Rus and confirmed that the particles without phosphonate modification showed limited cellular

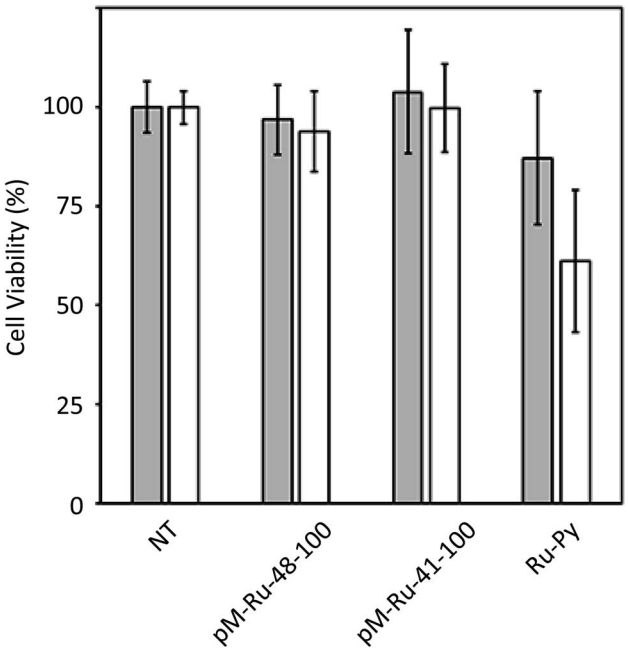

Fig. 3 Photo-induced cytotoxicity of pM-Rus and Ru–Py against HeLa cells. After the cells were incubated for 24 h in the presence of pM-Rus (0.02 mg mL^{-1}) and Ru–Py (10 μM), the cells were irradiated (450 nm) for 0 (gray) or 20 min (white). Cell viability was calculated by using a cell counting kit-8 (WST-8). NT means no treatment. Results are shown as the mean ± SD ($n = 5$).

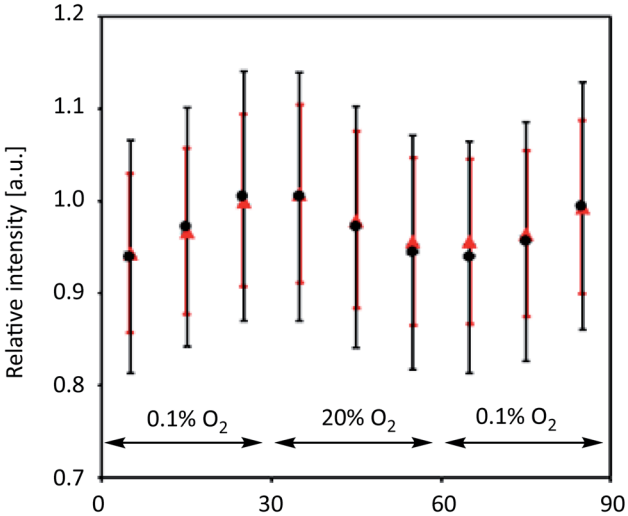

Fig. 4 Change in phosphorescence intensity of pM-Ru-48-100 (black circle) and pM-Ru-41-100 (red triangle) in the cells. The cells were incubated under different oxygen conditions. The oxygen concentration of the medium was changed every half hour (0–30 min: 0.1% O_2, 30–60 min: 20% O_2, 60–90 min: 0.1% O_2).

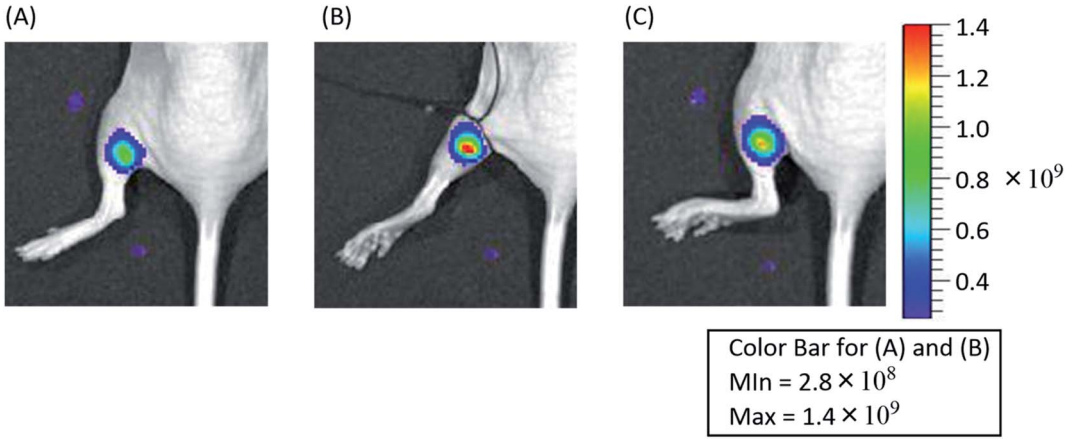

Fig. 5 Optical imaging of ischemia-based hypoxia *in vivo*. After pM-Ru-48-100 were injected intramuscularly into the left leg, emission was monitored by an *in vivo* imaging system (excitation at 465 nm, emission at 620 nm) (A). A hypoxic state was induced in the left leg by ligature, and the emission was monitored (B). Reperfusion was achieved by release of the ligature (C).

uptake (Fig. 2D). These findings indicate that their relatively large hydrophilic surface was responsible for cellular uptake.

We next evaluated the photo-induced cytotoxicity of pM-Rus of size 100 nm. A Ru complex reported previously, Ru–Py (Fig. S7†), which was not tethered to nanoparticles, was used as a control, and we compared the cytotoxic effects of pM-Rus and Ru–Py. As shown in Fig. 3, pM-Ru-48-100 and pM-Ru-41-100 of size 100 nm showed negligible toxicity toward HeLa cells even upon photoirradiation for 20 min. In contrast, the Ru–Py complex was significantly toxic to cells under photoirradiation conditions. We also evaluated the generation of $^1O_2$ in cells using singlet oxygen sensor green (SOSG), a fluorescent indicator of $^1O_2$. SOSG was administered to cells that had been treated with pM-Rus, and then the cells were photoirradiated. The bright emission of SOSG was observed from all of the cells incubated with pM-Rus (Fig. S8†), indicating that $^1O_2$ was generated in the cells. It is well known that the diffusion sphere of singlet oxygen is related to its lifetime.[32] In our previous research, singlet oxygen generated in the pores of the MSNs exhibited a short lifetime,[28] and therefore they were quenched within the pores before leaching out. Thus, pM-Rus showed negligible cytotoxicity upon photoirradiation, even when $^1O_2$ was generated. On the other hand, the Ru–Py complex showed toxicity upon photoirradiation. Ru–Py generated dispersed $^1O_2$, which damaged cellular molecules directly, because Ru–Py was dispersed in the cells. In light of these results, pM-Ru-48-100 and pM-Ru-41-100 were considered to be suitable for sensing oxygen.

We next assessed whether oxygen fluctuations in the cells could be monitored. For this purpose, we selected pM-Ru-48-100 and pM-Ru-41-100 to be incubated in HeLa cells under hypoxic or normoxic conditions (Fig. 4). When the cells were incubated under hypoxic conditions, an enhancement of emission at 612 nm was observed. In contrast, subsequent incubation under normoxic conditions decreased the emission intensity. The emission intensity continued to rise and fall according to the change in the oxygen levels in the cells. However, the relative phosphorescence seems changing 30 min later after each change of oxygen concentration of medium. Given that the phosphorescence intensity of ruthenium complexes changed instantaneously along with the concentration change of their surrounding environments, we assumed that the change of cellular oxygen concentration take a fair amount of time after change of oxygen concentration of medium. Thus, these results indicate that the emission of pM-Rus mirrors the oxygen fluctuation in the cells in real time. Further attempts were made to detect oxygen levels *in vivo* by pM-Rus. Among the particles prepared in the present study, pM-Ru-48-100 seems to show preferable properties for biological oxygen-imaging due to its high cellular uptake, good sensitivity toward molecular oxygen, and low cytotoxicity. Considering these observations, we used pM-Ru-48-100 to characterize its usefulness for *in vivo* imaging. After intramuscular injection of the particles into the left leg of nude mice, blood flow was reduced by ligating the left leg under anesthesia to create a hypoxic region. As shown in Fig. 5, the emission intensity in the left leg was enhanced after ligation. Conversely, release of the ligature and reperfusion led to re-oxygenation, resulting in a decrease in emission intensity. Thus, it is reasonable to conclude that pM-Rus are a promising indicator of oxygen levels *in vivo*.

Conclusion

In summary, we prepared phosphonated-mesoporous nanoparticles bearing Ru complexes in their pores (pM-Rus), and characterized their properties as oxygen-sensing probes. MCM-41- and MCM-48-type MSNs were synthesized and effectively tethered to Ru complexes in their pores. Each pM-Rus was smaller and showed better dispersity in aqueous solutions than a larger conventional probe, MSN-Ru. The pM-Rus showed robust phosphorescence emission that was dependent on the oxygen concentration. The K_{SV} values of pM-Rus were higher than those of MSNs without phosphonate modifications,

indicating that they had high sensitivity toward molecular oxygen. Cellular experiments revealed that the pM-Rus material of size 100 nm had negligible cytotoxic effects even under photoirradiation conditions due to the deactivation of $^1O_2$ before leaching out of the pores. Animal experiments revealed that pM-Ru provides robust emission in a hypoxic region created in a mouse leg. Thus, pM-Rus are promising probes for detecting oxygen levels *in vivo*.

In this study, we successfully prepared size-controlled and hydrophilic nanoparticles. These molecular probes can be applied to visualization of tumor hypoxia, because accumulation of nanoparticles in tumor tissue is affected by their size. Further application of these probes to the optical imaging of oxygen levels in tumor tissues is in progress.

Experimental section

Materials and methods

1,10-Phenanthroline maleimide, ethanol (99.5), hexadecyltrimethylammonium bromide (CTAB), disodium hydrogen phosphate, sodium dihydrogen phosphate dihydrate, Dulbecco's modified minimum essential medium (DMEM), and Dulbecco's phosphate buffer saline (PBS) were purchased from Nacalai Tesque Inc. (Kyoto, Japan). *cis*-Dichlorobis(2,2′-bipyridine)ruthenium(II) dehydrate, NaOH aq. (2.0 M) and *N*,*N*-dimethylformamide were purchased from FUJIFILM Wako Pure Chemical Industries (Osaka, Japan). Pluronic F-127, triethanolamine (TEA), 3-(trihydroxysilyl)propyl methylphosphonate monosodium salt solution 50 wt% in H_2O (THMP), (3-mercaptopropyl)-triethoxysilane (MPTS), fetal bovine serum (FBS), trypsin–EDTA, penicillin, and streptomycin were purchased from Sigma-Aldrich Japan K.K (Tokyo, Japan). Ammonia solution (28 wt%) and tetraethylorthosilicate (TEOS) were purchased from Tokyo Chemical Industry (Tokyo, Japan). A cell counting kit-8 was purchased from Dojindo Laboratories (Kumamoto, Japan). Bis(2,2′-bipyridine)(5-maleimide-1,10-phenanthroline)ruthenium(II) was prepared as described previously.[18] All reagents were used without further purification unless otherwise stated. Xenogen *in vivo* Imaging System (IVIS; Xenogen) were used for *in vitro* and *in vivo* phosphorescence imaging studies. BALB/c nu/nu mice were purchased from SLC (Shizuoka, Japan). The mice were housed at the Institute of Laboratory Animals at Kyoto University Graduate School of Medicine. All studies and procedures were approved by Animal Research Committee of Kyoto University Graduate School of Medicine. All animal experiments were performed according to the Institutional Guidance of Kyoto University on Animal Experimentation and under permission by the animal experiment committee of Kyoto University.

Synthesis of MCM-41-type mesoporous silica nanoparticles of size 100 nm

MCM-41-type mesoporous silica nanoparticles were synthesized following the previously reported method.[31] Briefly, CTAB (0.5 g) was dissolved in H_2O (125 mL), 2.0 M NaOH, and the mixture was heated at 80 °C for 1 h. After the slow addition of TEOS (1.5 mL), the solution was further heated and stirred at 80 °C for 2 h. The resulting white solution was then centrifuged at 20 000 rcf × 20 min, and washed twice with water and twice with EtOH. The precipitant was dried in air overnight. Next, the particles were calcined at 550 °C for 5 h (air, heating rate 1 °C min^{-1}).

Synthesis of MCM-48-type mesoporous silica nanoparticles of size 100 nm

MCM-48-type mesoporous silica nanoparticles were synthesized following the previously reported method with some modification.[30] Briefly, CTAB (0.5 g) and F-127 (4.0 g) were dissolved in EtOH (33.7 mL) and 2.9 wt% NH_4OH solution (106.6 mL) and stirred overnight at 25 °C under a high stirring rate (1000 rpm). Next, TEOS (1.8 mL) was added and the mixture was stirred for 1 min. The reaction mixture was then aged for 24 h under static conditions (air, RT). The resulting product was collected by centrifugation (20 000 rcf, 20 min), washed twice with water and once with EtOH, and dried overnight in air. The particles were then calcined at 550 °C for 5 h (air, heating rate 1 °C min^{-1}).

Synthesis of MCM-48-type mesoporous silica nanoparticles of size 50 nm

MCM-48 silica nanoparticles of size 50 nm were synthesized as reported in the literature.[30] Briefly, CTAB (331.6 mg), F127 (1.34 g) and triethanolamine (TEA) (7.82 g) were dissolved in EtOH (28.5 mL) and water (62.5 mL) and stirred overnight at 1000 rpm in a polypropylene (PP) bottle at room temperature. Next, TEOS (1.28 mL) was added in one shot at 25 °C under a high stirring rate (1000 rpm) for 1 min. The reaction mixture was then aged for 24 h under static conditions (air, RT). After 24 h, 100 mL of ethanol was added and the resulting product was collected by ultracentrifugation (40 000 rpm, 25 min), washed twice with water and once with EtOH, and dried overnight in air. The particles were then calcined at 550 °C for 5 h (air, heating rate 1 °C min^{-1}).

Thiol modification of MSNs

100 mg of all of the calcined MSNs was dried in 100 °C under vacuum overnight and dispersed in 10 mL of dry toluene. The solution was refluxed for 1 h. MPTS (0.1 mL) was added and the mixture was further refluxed overnight. The resulting solution was centrifuged (7200 rcf, 10 min), washed three times with ethanol and twice with water, and lyophilized overnight.

Double functionalization of MSNs

All of the as-synthesized MSNs before calcination, containing surfactant micelles in their pores, were dispersed in water (100 mg in 13 mL water). THMP (0.13 mL) was dissolved in water (13 mL), and the pH of this solution was adjusted to pH 5. This solution was added to an MSN suspension and refluxed at 100 °C overnight. The obtained surface-phosphonated MSNs were purified by centrifugation (7200 rcf, 10 min), and washed three times with water and twice with EtOH.

To remove the surfactant, the phosphonated MSNs were dispersed in ethanol (100 mg in 20 mL of EtOH) and HCl (5 mL).

The dispersion was sonicated, refluxed for 1 h, and then centrifuged (7200 rcf, 10 min). This process was repeated three times and the mixture was washed twice with EtOH and dried under vacuum overnight. The removal of surfactant was confirmed by physisorption and thermogravimetric analysis.

The resulting particles were dried under vacuum at 100 °C overnight. The particles were dispersed in dry toluene (100 mg in 10 mL toluene), and refluxed under Ar for 2 h. MPTS (0.1 mL) was added and the mixture was further refluxed overnight. The resulting dispersion was centrifuged (7200 rcf, 10 min), washed three times with ethanol and twice with water, and lyophilized overnight.

Insertion of the ruthenium complexes into MSNs

Functionalized MSNs (27 mg) and bis(2,2′-bipyridine)(5-maleimide-1,10-phenanthroline)ruthenium(II) (27.4 mg, 39.8 μmol) were dissolved in DMF (1.5 mL) containing 1.5 mL phosphate buffer (pH 8.4), and the resulting mixture was stirred for 12 h at room temperature in the dark. After the reaction, the mixture was washed with ethanol and water, and centrifuged (5000 rcf, 5 min). Washing of the precipitate with water (×10) and lyophilization gave MSN-Ru or pMSN-Ru as a brownish orange solid (48.7 mg, 90%). The formation of each M-Rus and pM-Rus was confirmed by measurement of luminescent spectra. The amount of ruthenium complex introduced in MSNs was measured by atomic absorption spectra (AAS), with the dispersion in 1 M aqueous HCl solution.

Measurement of phosphorescent spectra

Phosphorescence spectra were measured with pM-Rus and M-Rus (0.02 mg mL^{-1}) in PBS containing 1% DMSO. All phosphorescence spectra were recorded on a JASCO EF-6300 spectrofluorophotometer with a 1 cm quartz cell.

DLS and zeta potential

Stable aqueous suspensions of the material (0.7 mg mL^{-1}) were obtained by performing three cycles of vortex shaking (10 min) and ultrasonic bath treatment (20 min). The supernatant was then analyzed to determine hydrodynamic diameters and zeta potential values using a Malvern Zetasizer Nano ZS. Measurements were accepted as valid only when satisfactory quality criteria such as polydispersity index and steepness of the correlogram function were fulfilled.

Thermogravimetric analysis

Thermogravimetric analysis was conducted from room temperature to 800 °C with a heating rate of 10 °C min^{-1}. An air flow of 20 mL min^{-1} and additional protective N_2 flow of 20 mL min^{-1} were used. The percentage of grafted moieties was calculated based on the detected mass loss between 150 °C and 800 °C. This analysis was performed using a Thermo plus EVO II TG-DTA (Rigaku).

Nitrogen physisorption analysis at −196 °C

Prior to the measurements, the samples were outgassed under vacuum overnight at 80 °C for functionalized particles. The specific surface area (S_{BET}) was obtained using the BET equation in the range of 0.05–0.15P/P_0. The total pore volume was determined at $P/P_0 = 0.95$ according to the Gurvitch rule, and the pore-size analysis was performed using the NLDFT model, assuming a cylindrical pore geometry and a silica surface. Calculations were performed with AsiQwin software v.5.0 provided by Quantachrome. This analysis was performed with a Quantachrome iQ3 instrument (Anton Paar, Boynton Beach, FL, USA).

Transmission electron microscopy and energy dispersive X-ray spectroscopy

The nanoparticles were dispersed in water by using an ultrasonic bath and further deposited on a carbon-coated copper microgrid. Images were obtained with a JEM-1400 (JEOL) at an accelerating voltage of 120 kV in bright-field mode. EDX images were obtained at an accelerating voltage of 100 kV.

Powder X-ray diffraction

Low-angle diffractograms of MSNs were recorded on a PANalytical Empyrean diffractometer (Malvern PANanalytical, UK) in reflection geometry (Bragg–Brentano HD) using Cu Kα1+2 radiation at a voltage of 45 kV, a tube current of 40 mA, and a fixed divergence slit of 0.05 mm. Measurements were performed in continuous mode with a step size 2θ of 0.013° and a time per step of 300 s. The low-angle XRD pattern of sample PXI-3 was recorded in transmission geometry in continuous mode with a step size 2θ of 0.013°, a time per step of 250 s, and with a fixed divergence slit of 0.76 mm.

Determination of K_{SV} values

0.02 mg of pM-Rus or M-Rus was dispersed in 1 mL of 1% DMSO/PBS solution. These samples (100 μL) were incubated in a 96-well black plate and their phosphorescence was measured with a TECAN Spark M10 microplate reader under a changing oxygen pressure (20%, 10%, 5%, 2% and 0.1%).

The Stern–Volmer coefficient (K_{SV}) of each M-Ru and pM-Ru was estimated by using the following equation:

$$I_0/I = 1 + K_{SV}[O_2]$$

where I_0 is the relative emission intensity at 0.1% O_2, I is the emission intensity at arbitrary O_2 concentrations, and K_{SV} is the Stern–Volmer coefficient. A Stern–Volmer plot ($[O_2]$ *versus* $[I_0/I]$) was used to determine the K_{SV} value.

Cell culture

HeLa cells were cultured at 37 °C in 5% CO_2 in 75 cm^2 flasks containing Dulbecco's modified minimum essential medium (DMEM) supplemented with 10% fetal bovine serum (FBS), 1% 10 000 U mL^{-1} penicillin and 10 mg mL^{-1} streptomycin.

Cytotoxic effect of pM-Rus and molecular phosphorescent probes (Ru–Py)

To HeLa cells (1.0×10^3 cells per cm^3) cultured in 96-well plates for 24 h, pM-Ru-48-100, pM-Ru-41-100 (0.02 mg mL^{-1}) or Ru–Py (10 μM) were added and the cells were then incubated for 24 h at 37 °C. After being washed, living cells were stained by WST-8 and the absorbance at 450 nm was measured by a iMark Microplate reader (Bio Rad Laboratories, Inc., Hercules, CA, USA). To evaluate the cytotoxic effect under photoirradiation conditions, cells were irradiated with 450 nm light for 20 min after the addition of pM-Rus or Ru–Py, and the cells were washed. After 2 h incubation, living cells were then stained by WST-8 and the absorbance at 450 nm was measured.

Cellular imaging

To HeLa cells (3.0×10^4 cells) cultured in 35 mm glass-bottom dishes for 24 h, pM-Ru (0.02 mg mL^{-1}) was added and the cells were incubated for 24 h at 37 °C. After incubation, phosphorescent images were obtained by confocal microscopy (LSM 710, Carl Zeiss). Phosphorescent images were acquired using an argon laser (458 nm) for excitation and a 600–700 nm band-pass filter for emission. The specimens were viewed with a confocal laser-scanning microscope at high magnification using a 63× oil objective.

Cellular uptake of nanoparticles

HeLa cells (2.0×10^5 cells per cm^2) were seeded on a 6-multi-well cell culture plate and incubated for 24 h at 37 °C. After the addition of nanoparticles, the cells were further incubated for 24 h at 37 °C. Next, the cells were washed with PBS and peeled off by trypsin EDTA. After the cell membranes were destroyed by the addition of nitric acid (1 M, including Triton at 1%), the concentration of ruthenium complexes was determined by ICP measurements (iCAP 7400 ICP-OES, Thermo Fisher Scientific, Tokyo, Japan).

Imaging of oxygenation and deoxygenation of HeLa cells

Visualization of the oxygenation and deoxygenation of HeLa cells was performed on a plate reader (Tecan Spark 10M) with excitation at 450 nm and emission at 612 nm. HeLa cells (2.5×10^5 cells) were incubated with pM-Ru-48-100 (0.02 mg mL^{-1}) or pM-41-100 (0.02 mg mL^{-1}) for 24 h at 37 °C. After the cells had been washed, the emission intensity at 600 nm from the cells in Fluoro-Bright DMEM (Gibco) was measured. After this first measurement, the medium was replaced by FluoroBright DMEM and then the cells were incubated under hypoxic (0.1% O_2) or normoxic (20% O_2) conditions. The emission intensity was measured every 10 minutes during incubation.

Detection of singlet oxygen generation in the cells

HeLa cells (3.0×10^4 cells) were seeded in 35 mm glass-bottom dishes and cultured for 24 h at 37 °C. pM-Ru-48-100 and pM-Ru-41-100 (0.02 mg mL^{-1}) were added and the cells were incubated for 24 h at 37 °C. To stain singlet oxygen, Singlet Oxygen Sensor Green (SOSG, 2.5 μM) was added after washing out of excess pM-Rus, and the cells were further incubated for 3 h. After the cells were washed, they were irradiated for 10 min with 450 nm light and fluorescent images of SOSG were acquired using 488 nm excitation and a 500–525 nm filter.

In vivo imaging using nude mice

Before scanning, female BALB/cSlc-nu/nu mice weighing ~20 g were anesthetized, and then pM-Ru-48-100 (1 mM, 10 μL) were intramuscularly injected into the left leg. The left leg was then ligated by a band. After 3 min, whole-body images were acquired (excitation at 465 nm, emission at 620 nm). The ligature was then released and we observed whole-body images.

Conflicts of interest

There are no conflicts to declare.

Acknowledgements

This work was supported in part by a Grant-in-Aid for Scientific Research (for K. T., grant number 20H02863, and T. K., 18K05353) and a Grant-in-Aid for JSPS Fellows (for Y. U., grant number 17J03866). F. K. acknowledges funding support from the University of Vienna, Austria.

References

1 H. Kurokawa, H. Ito, M. Inoue, K. Tabata, Y. Sato, K. Yamagata, S. Kizaka-Kondoh, T. Kadonosono, S. Yano, M. Inoue and T. Kamachi, *Sci. Rep.*, 2015, **5**, 1–3.
2 R. D. Braun, J. L. Lanzen and M. W. Dewhirst, *Am. J. Physiol.: Heart Circ. Physiol.*, 1999, **277**, 551–568.
3 J. Lanzen, R. D. Braun, B. Klitzman, D. Brizel, T. W. Secomb and M. W. Dewhirst, *Cancer Res.*, 2006, **66**, 2219–2223.
4 G. L. Semenza, *Annu. Rev. Med.*, 2003, **54**, 17–28.
5 G. L. Semenza, *Trends Mol. Med.*, 2001, **7**, 345–350.
6 C. Murdoch, M. Muthana and C. E. Lewis, *J. Immunol.*, 2005, **175**, 6257–6263.
7 A. L. Harris, *Nat. Rev. Cancer*, 2002, **2**, 38–47.
8 P. Vaupel, F. Kallinowski and P. Okunieff, *Cancer Res.*, 1989, **49**, 6449–6465.
9 K. Tanabe, N. Hirata, H. Harada, M. Hiraoka and S. I. Nishimoto, *ChemBioChem*, 2008, **9**, 426–432.
10 E. Nakata, Y. Yukimachi, H. Kariyazono, S. Im, C. Abe, Y. Uto, H. Maezawa, T. Hashimoto, Y. Okamoto and H. Hori, *Bioorg. Med. Chem.*, 2009, **17**, 6952–6958.
11 K. Kiyose, K. Hanaoka, D. Oushiki, T. Nakamura, M. Kajimura, M. Suematsu, H. Nishimatsu, T. Yamane, T. Terai, Y. Hirata and T. Nagano, *J. Am. Chem. Soc.*, 2010, **132**, 15846–15848.
12 H. Komatsu, K. Tanabe and S. I. Nishimoto, *Bioorg. Med. Chem. Lett.*, 2011, **21**, 790–793.
13 K. Okuda, Y. Okabe, T. Kadonosono, T. Ueno, B. G. M. Youssif, S. Kizaka-Kondoh and H. Nagasawa, *Bioconjugate Chem.*, 2012, **23**, 324–329.

14 E. Lopci, I. Grassi, A. Chiti, C. Nanni, G. Cicoria, L. Toschi, C. Fonti, F. Lodi, S. Mattioli and S. Fanti, *Am. J. Nucl. Med. Mol. Imaging*, 2014, **4**, 365–384.
15 Z. Rosenzweig and R. Kopelman, *Anal. Chem.*, 1995, **67**, 2650–2654.
16 K. Tanabe, H. Harada, M. Narazaki, K. Tanaka, K. Inafuku, H. Komatsu, T. Ito, H. Yamada, Y. Chujo, T. Matsuda, M. Hiraoka and S. I. Nishimoto, *J. Am. Chem. Soc.*, 2009, **131**, 15982–15983.
17 S. Iwaki, K. Hanaoka, W. Piao, T. Komatsu, T. Ueno, T. Terai and T. Nagano, *Bioorg. Med. Chem. Lett.*, 2012, **22**, 2798–2802.
18 H. Komatsu, K. Yoshihara, H. Yamada, Y. Kimura, A. Son, S. I. Nishimoto and K. Tanabe, *Chem.–Eur. J.*, 2013, **19**, 1971–1977.
19 A. Son, A. Kawasaki, D. Hara, T. Ito and K. Tanabe, *Chem.–Eur. J.*, 2015, **21**, 2527–2536.
20 D. Hara, H. Komatsu, A. Son, S. I. Nishimoto and K. Tanabe, *Bioconjugate Chem.*, 2015, **26**, 645–649.
21 D. Hara, Y. Umehara, A. Son, W. Asahi, S. Misu, R. Kurihara, T. Kondo and K. Tanabe, *ChemBioChem*, 2018, **19**, 956–962.
22 S. Zhang, M. Hosaka, T. Yoshihara, K. Negishi, Y. Iida, S. Tobita and T. Takeuchi, *Cancer Res.*, 2010, **70**, 4490–4498.
23 T. Murase, T. Yoshihara and S. Tobita, *Chem. Lett.*, 2012, **41**, 262–263.
24 Y. Hirakawa, T. Yoshihara, M. Kamiya, I. Mimura, D. Fujikura, T. Masuda, R. Kikuchi, I. Takahashi, Y. Urano, S. Tobita and M. Nangaku, *Sci. Rep.*, 2015, **5**, 1–7.
25 A. V. Kondrashina, R. I. Dmitriev, S. M. Borisov, I. Klimant, I. O'Brien, Y. M. Nolan, A. V. Zhdanov and D. B. Papkovsky, *Adv. Funct. Mater.*, 2012, **22**, 4931–4939.
26 R. I. Dmitriev, A. V. Kondrashina, K. Koren, I. Klimant, A. V. Zhdanov, J. M. P. Pakan, K. W. McDermott and D. B. Papkovsky, *Biomater. Sci.*, 2014, **2**, 853–866.
27 T. Nakamura, A. Son, Y. Umehara, T. Ito, R. Kurihara, Y. Ikemura and K. Tanabe, *Bioconjugate Chem.*, 2016, **27**, 1058–1066.
28 N. Kitajima, Y. Umehara, A. Son, T. Kondo and K. Tanabe, *Bioconjugate Chem.*, 2018, **29**, 4168–4175.
29 N. Hoshyar, S. Gray, H. Han and G. Bao, *Nanomedicine*, 2016, **11**, 673–692.
30 M. Bouchoucha, M. F. Côté, R. C-Gaudreault, M. A. Fortin and F. Kleitz, *Chem. Mater.*, 2016, **28**, 4243–4258.
31 R. Guillet-Nicolas, J. L. Bridot, Y. Seo, M. A. Fortin and F. Kleitz, *Adv. Funct. Mater.*, 2011, **21**, 4653–4662.
32 J. Moan, *J. Photochem. Photobiol., B*, 1990, **6**, 343–347.